*Asian Journal of Water, Environment and Pollution,* Vol. 21, No. 6 (2024), pp. 49-57.
DOI 10.3233/AJW240072

# Study of Operating Parameters on the Optimum Hydrogen Yield Through the Ethanol Steam Reforming

**Aamir Baig, Vibha Goswami[1] and Sonal***

Department of Chemical Engineering, Malaviya National Institute of Technology Jaipur, Rajasthan – 302017, India
[1]Central Institute of Petrochemical Engineering and Technology, IPT Jaipur, Rajasthan – 302017, India
✉ sonal.chem@mnit.ac.in

*Received May 12, 2024; revised and accepted June 17, 2024*

**Abstract:** This work presents a detailed study of the effects of reaction parameters on the 7.5Ni-7.5La/Ce-Zr catalyst in catalytic steam reforming of ethanol (SRE). The study of the collective effect of reaction parameters on the product yield will help to design an efficient catalyst system for the reforming process. The catalyst morphology and properties were analysed by different techniques such as FESEM, XRD, BET, and TPR. The catalyst activity test was performed in a tubular reactor with different S/C ratios, temperatures, and flow rates. The catalyst showed an optimum hydrogen yield (3.8) and ethanol conversion (98 %) at a S/C ratio of 4.5, a feed flow rate of 2.5 g/gcat-h, and a temperature of 600 °C. The exit flow rate of $H_2$ is found to be 10 mmol/min at the same reaction condition. The present catalyst shows superior catalytic performance and resistance to carbon deposition during SRE.

**Key words:** Steam reforming, hydrogen yield, Ni-based catalyst, ethanol conversion.

## Introduction

The demand for clean alternative energy sources with high energy efficiency steadily rises as fossil fuel resources become depleted. Concerns about the finite supply of fossil fuels and their environmental effects have led to a significant increase in scientific interest in hydrogen (Abd El-Hafiz and Ebiad, 2015). This fuel alternative's carbon-free nature and high energy density have made it one of the most promising options. At 120.7 kJ/g, hydrogen, which is extensively distributed across the universe, has the highest energy content per unit of weight, surpassing all known fuels. However, around 95% of $H_2$ is currently derived from other sources (Vizcaíno et al., 2007). However, issues with distributing, storing, and transporting hydrogen still raise serious questions about supply and safety. On-board reformers and liquid fuels as hydrogen transporters appear promising as a temporary fix. It is the most advantageous choice for producing hydrogen when compared to hydrocarbon fuels (Frusteri et al., 2004).

Reforming ethanol via steam has gained popularity due to the effective yield of $H_2$ and the technique for manufacturing ethanol from bio-resources. It emerges as an enticing solution for hydrogen supply in fuel cells, such as PEM types, avoiding safety and storage concerns (Ni et al., 2007). Additionally, SRE aims to maximise hydrogen yield by capturing hydrogen from ethanol and water. Several catalysts, predominantly nickel, lanthanum, and noble metals-based, have been documented for SRE (Li et al., 2010).

The catalyst containing nickel is preferred for its ability to withstand carbon deposition (C-C) and its

*Corresponding Author

affordability. Carbon deposition and the sintering of nickel particles at ESR reaction conditions are two factors that lead to the deactivation of catalysts based on nickel. Nevertheless, few catalysts are susceptible to significant carbon formation under actual reaction conditions (Phaahlamohlaka et al., 2017). Numerous studies have investigated noble catalysts to address the deposition of carbon (Sanchez-Sanchez et al., 2010). Among various supports, those based on $CeO_2$ are favoured due to the property of ceria to store oxygen (Xiao et al., 2021). Under certain conditions, $CeO_2$-$ZrO_2$ exhibits redox characteristics due to lattice deformation and charge imbalance. This property promotes the oxidation of undesirable carbonaceous compounds on the surface of the catalyst.

In addition, several techno-economic analyses of the reforming process suggest that nickel is the most economically feasible catalyst in comparison to other transition and noble metals (Co, Cu Pt, Pd, etc.) used for the reforming process (Alptekin and Celiktas, 2022). Several reports suggest the industrial-scale application of Ni-based catalysts with the least environmental impacts.

Some prominent parameters affect the yield of hydrogen and ethanol conversion significantly. The operating conditions that affect the hydrogen yield and feed conversion are temperature, the S/C ratio, and feed flow rates. Steam promotes the equilibrium favoring hydrogen production. Nonetheless, it's important to note that the S/C ratio cannot be increased indefinitely within a process (Quan et al., 2017). Hydrogen yield was obtained as 3.8 mol $H_2$ per mol ethanol with catalyst Cu-Ni/La20-SBA at ethanol to water molar ratio of 3.7 at 600$^o$C (Calles et al., 2009). At the ethanol-water molar ratio of 6, the hydrogen yield was obtained at 1.8 with the catalyst Ni/$SiO_2$ (Liu et al., 2016). They propose that an increased presence of $H_2O$ molecules occupies catalysts' reactive sites, preventing the absorption of ethanol molecules. The variations in the molar flow rates of the reactants exert a substantial influence on both the reaction's efficiency and the resultant product distribution.

In the current study, the effect of parameters like S/C ratio, temperature, and flow rates of feed on Ni-La doped ceria-zirconia catalyst characteristics have been studied to understand their effect on hydrogen yield and ethanol conversion. Collectively, this innovative catalyst configuration represents promising prospects for the impact of parameters on hydrogen reforming. The range of the experimental parameters has been selected based on the reported reforming papers. The experiments were conducted in the industrial relevant reaction condition ranges viz. temperature 400°C - 700°C, feed flow rate:0.8 to 4 g/gcat-h, and steam to carbon (S/C ) molar ratio:1.5 to 9 (Mortensen and Dybkjær, 2015)

## Material and Experimental Methods

### Catalyst Preparation

The Ce-Zr support was prepared by the coprecipitation process with an equal weight ratio of 1:1, followed by the wetness impregnation method. Metal nitrates $Ni(NO_3)_2.6H_2O$, $La(NO_3)_2.6H_2O$, $Ce(NO_3)_2.6H_2O$, and$Zr(NO_3)_2.6H_2O$ were used as precursors. Adding the weighed quantity of Ce-Zr precursor to deionised water, the mixture was agitated at 70°C for an hour. Increasing the pH to 10 would help the metal hydroxides precipitate, liq. $NH_3$ was added. To create mixed oxides of $CeO_2$-$ZrO_2$, the filtrate was dried at 120$^o$C and then calcined at 550 $^o$C for 6 hours. The Ni and La were impregnated on the prepared support $CeO_2$-$ZrO_2$ by rotary evaporator for uniform mixing, and drying and calcination of the catalyst occurred at 550$^o$C for 6 hours. Finally, the catalyst is prepared as 7.5Ni-7.5La/ $CeO_2$-$ZrO_2$.

### Reactor Set up

A tubular reactor constructed from MOC-Inconel, featuring an ID=2 cm, L= 30 cm, was furnished with 3 grams of catalyst particles. Gas cylinders containing $H_2$ and $N_2$ were linked to the reactor inlet, with mass flow controllers ensuring precise regulation and delivery of gases to the catalyst bed. The catalyst underwent a reduction before starting the reaction at 550°C for 5 hours in the presence of $H_2$ at a flow rate of 30 ml/min. The outlet product containing unreacted gases which are analysed by GC, for thermal conductivity detector (TCD) having Hayesep-Q column and for flame Ionised detector (FID) having Porapak-Q column.

Ethanol conversion is defined as a mole of ethanol converted per mole of ethanol-fed.$H_2$yield is defined as the ratio of the mole of $H_2$ produced to the mole of ethanol reacted, and feed flow rate is defined as weight hourly space velocity (WHSV) based on ethanol flow having unit g/gcat-h. All the experiments are conducted for 12 hours, and steady-state data are reported.

### Catalyst Characterisation

The characterization of the catalyst was performed using various methods such as PXRD, HRTEM, FESEM, BET, and TPR.

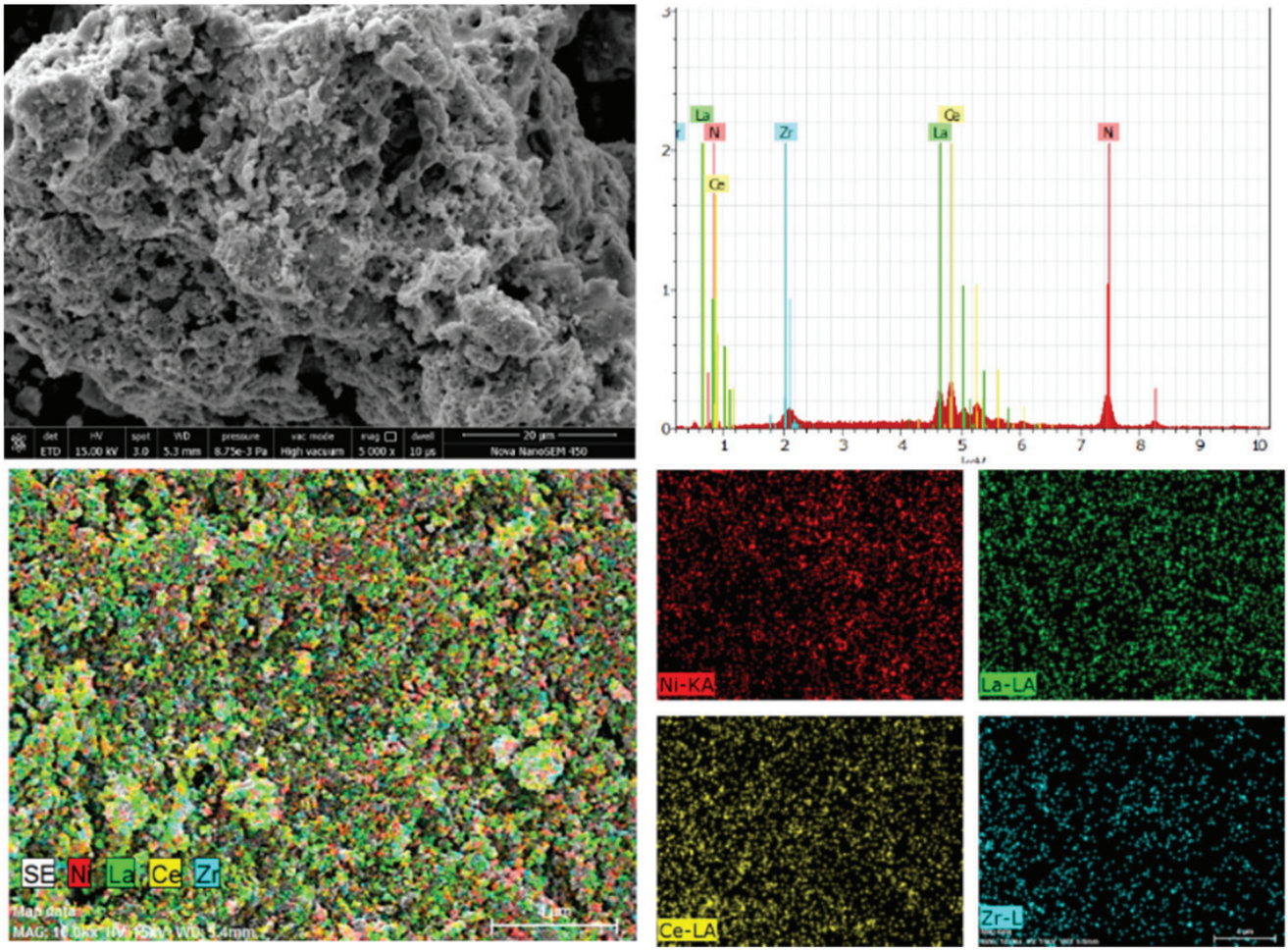


**Figure 1: FESEM Images and EDS spectra of fresh 7.5Ni-7.5La/$CeO_2$-$ZrO_2$ catalyst.**

## Results and Discussion

### Catalyst Characterisation

The atomic distribution and mass percentage of the 7.5Ni-7.5La/Ce-Zr catalyst surface were determined using the SEM-EDS analysis as shown in Figure 1. On the surface of the Ce-Zr support, Ni and Lanthana were discovered, with the relative % distribution of these components as shown in Table 1.

The crystal structure of the 7.5Ni-7.5La/$CeO_2$-$ZrO_2$ catalyst was analysed using X-ray analysis. JCPDS No. (96-900-9009) identify the characteristic peaks at 2θ = 33 °, 47.6 °, 56 °, 76.7 ° shows the $CeO_2$ phase. The $ZrO_2$ displayed diffraction peaks at 2θ = 34.22°, 49.32°; the values were verified by the pure phase of $ZrO_2$ with (JCPDS No.96-210-8456). All the characteristic peaks of 7.5Ni-7.5La/$CeO_2$-$ZrO_2$ catalyst correspond well with the NiO (JCPDS No. 96-152-6381) and $La_2O_3$(JCPDS No. (96-152-3969). The peaks of NiO at 2θ = 37.5°, 43.6°, 63° and a wide peak of $La_2O_3$ were visible at 2θ = 44.6°. Diffraction peaks of $CeO_2$ and $La_2O_3$ were observed at 2θ = 29° due to a similar diffraction angle as shown in Figure 2. The average crystal size of catalyst 7.5Ni-7.5La/$CeO_2$-$ZrO_2$ is calculated as 11.9 nm by the Scherrer equation.

**Table 1: Elemental analysis from EDS**

| *Catalyst* | *Initial wt % (taken while catalyst preparation)* | | | | *Observed*wt %* | | | |
|---|---|---|---|---|---|---|---|---|
| | *Ce* | *Zr* | *Ni* | *$La_2O_3$* | *Ce* | *Zr* | *Ni* | *La* |
| 7.5Ni-7.5La/Ce-Zr | 42.5 | 42.5 | 7.5 | 7.5 | 40.5 | 41.5 | 9.5 | 8.5 |

*Observed from EDS analysis

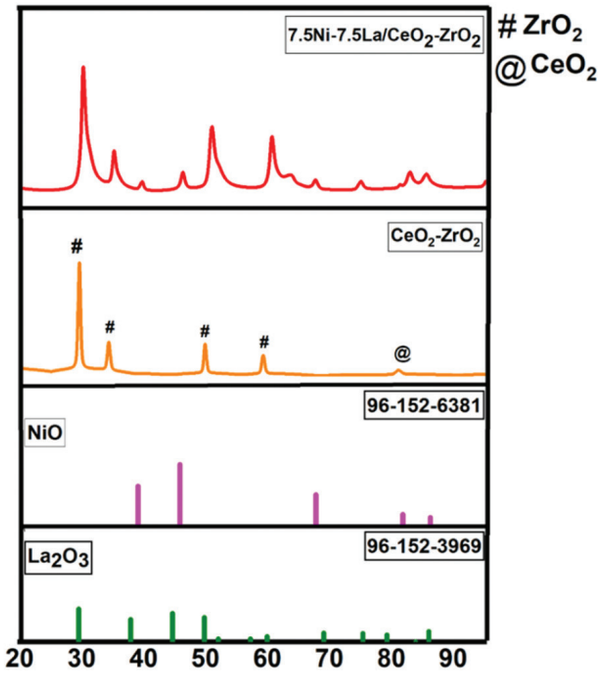


**Figure 2: XRD pattern of fresh calcined catalyst 7.5Ni-7.5La/$CeO_2$-$ZrO_2$.**

Figure 3 depicts the TPR analysis of 7.5Ni-7.5La/$CeO_2$-$ZrO_2$ catalyst is aimed at comprehending the reduction characteristics of Ni, La, $CeO_2$, and $ZrO_2$. The coexistence of various metal components and oxides may give rise to intricate interactions and synergistic effects, which can be uncovered via TPR analysis. There are three reduction peaks identified at temperatures 365°C, 400°C and 505°C. The reduction of ceria is aided by creating defect-related hydroxyl groups on ceria and forming vacancies (Trane-Restrup et al., 2013). The TPR profile of Nickel oxide reveals a peak at 365°C, indicating full reduction. There are two peaks identified which contain nickel. The peak found on these catalysts at 400°C suggested the reduction of NiO to metallic nickel NiO +$H_2$→ Ni + $H_2O$, as well as support reduction assisted by metal particle production. The $La_2O_3$ effect on support was also analyzed and concluded that the identical reduction profile for $La_2O_3$ and $CeO_2$ and quantitative studies for hydrogen consumption remain the same. The $La_2O_3$ is unreduced up to 800°C; hence the reduction peaks of $CeO_2$ and NiO overlapped, and quantifying the individual $H_2$ consumption attributed to each was challenging.

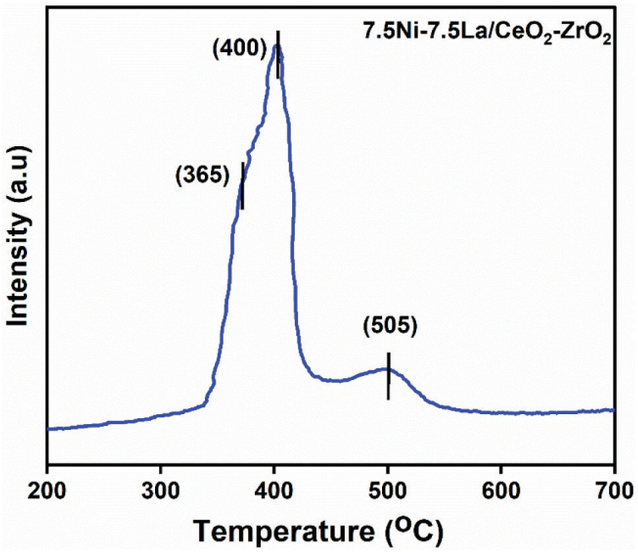


**Figure 3: TPR profiles of fresh calcined catalysts 7.5Ni-7.5La/$CeO_2$-$ZrO_2$.**

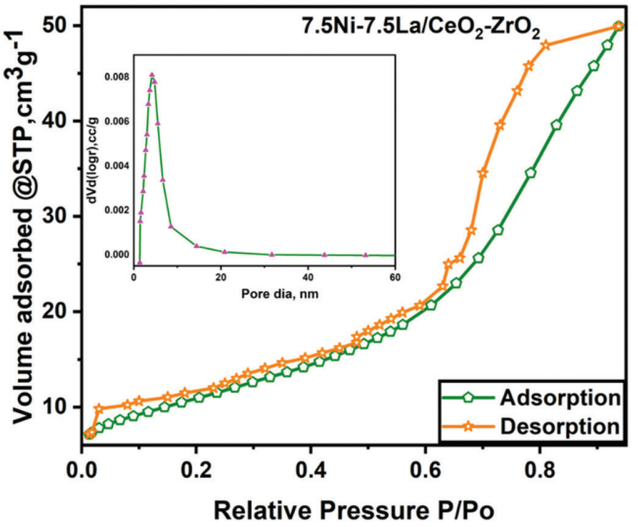


**Figure 4: BET adsorption-desorption curves and BJH pore-sized distribution curve for 7.5Ni-7.5La/ $CeO_2$-$ZrO_2$catalyst.**

The BET technique analyses the size of the pores, volume, and surface area of the prepared catalyst 7.5Ni-7.5La/$CeO_2$-$ZrO_2$. The surface area was found to be around 41 $m^2/g$ as shown in Table 2. Hence, Ce-Zr support for a higher surface area is desirable. Thus, mean pore diameter and pore volume were observed as 9.10 nm and 0.094 $cm^3/g$.

**Table 2: BET surface area, size of pores, and volume of pores of prepared catalyst**

| *Name of the catalyst* | *BET surface area ($m^2/g$)* | *Mean pore dia. (nm)* | *Pore volume ($cm^3/g$)* |
|---|---|---|---|
| 7.5Ni-7.5La/$CeO_2$-$ZrO_2$ | 41.10 | 9.10 | 0.094 |

The adsorption-desorption isotherm of the catalyst suggests the type IV hysteresis loop, indicating the mesoporous nature of the catalyst. The adsorption branch of the curve first rises strongly at low pressures as shown in Figure 4. This shows that gas molecules are adhering quickly to the catalyst's surface. The maximum volume adsorbed at 49 $cm^3g^{-1}$ at a relative pressure of 1. The desorption branch is often characterised by hysteresis, which occurs when the desorption curve does not coincide with the sorption curve. BJH plot observed the pore diameter and volume as 9 nm and 0.008cc/g. The pore volume of the $La_2O_3$ promoted catalyst significantly improved, consistent with the XRD results that demonstrated an expansion of the support lattice.

## Catalyst Activity Test

### Effect of Feed Flow Rate (WHSV)

The feed flow rate can substantially affect conversion and is regulated by numerous factors such as reaction kinetics and residence time. Reaction kinetics control how quickly ethanol and steam react to create hydrogen, carbon monoxide, and other products. The flow rate of the feed influences the residence time of reactants in the reactor. The ethanol feed flow was expressed in terms of weight hourly space velocity ($WHSV_{EtOH}$). The WHSV was varied from 0.8 to 4 g/gcat-h at 600 °C and 4.5 S/C molar ratio. Figure 5(a) shows that, as WHSV increases from 0.8 to 4 g/gcat-h, the ethanol conversion rate slightly increases from 88 to 96%. With the further increase in the flow rate, a decreasing trend was observed in conversion up to 93% due to the reduced residence time of feed with the catalyst bed. Shorter residence durations result from higher flow rates, which may reduce the time available for full conversion. An optimum ethanol conversion (96%) is achieved at a WHSV of 2.5 g/gcat-h. The maximum hydrogen yield is observed as 4.2 at the same optimum WHSV whereas the hydrogen yield slightly decreases on increasing the space velocity and reaches 3.4. Increased flow rates can expedite catalyst deactivation through mechanisms like heightened coke deposition or sintering of active sites, resulting in diminished hydrogen production efficiency over time.

Figure 5(b) shows that the exit flow rate of hydrogen also increases and reaches 14.3 mmole/min at a feed flow rate of 2.5 g/gcat-h. Similarly, as the $CO_2$ exit flow rate increases, increasing the flow rates of the ethanol/water mixture introduces a greater amount of water into the system, stimulating the water-gas shift reaction and consequently augmenting the $CO_2$ exit flow rate. The exit flow rate of CO ranges from 0.02 to 1.82 mmol/min. The reason for such a trend is that the water in the mixture encourages the WGS; that does not fully convert all CO to $CO_2$, particularly at higher flowrates where reaction kinetics could be constrained (Bej et al., 2017). A similar trend is followed in $CH_4$; it reaches a maximum of 2.9 mmol/min at a flow rate of 4.3 g/gact-h.

### Effect of Steam to Carbon (S/C) Ratio

Figure 6(a) shows that the S/C ratio increases from 1.5 to 9, and ethanol conversion also increases and reaches 96% at a ratio of 4.5. The fact for increasing

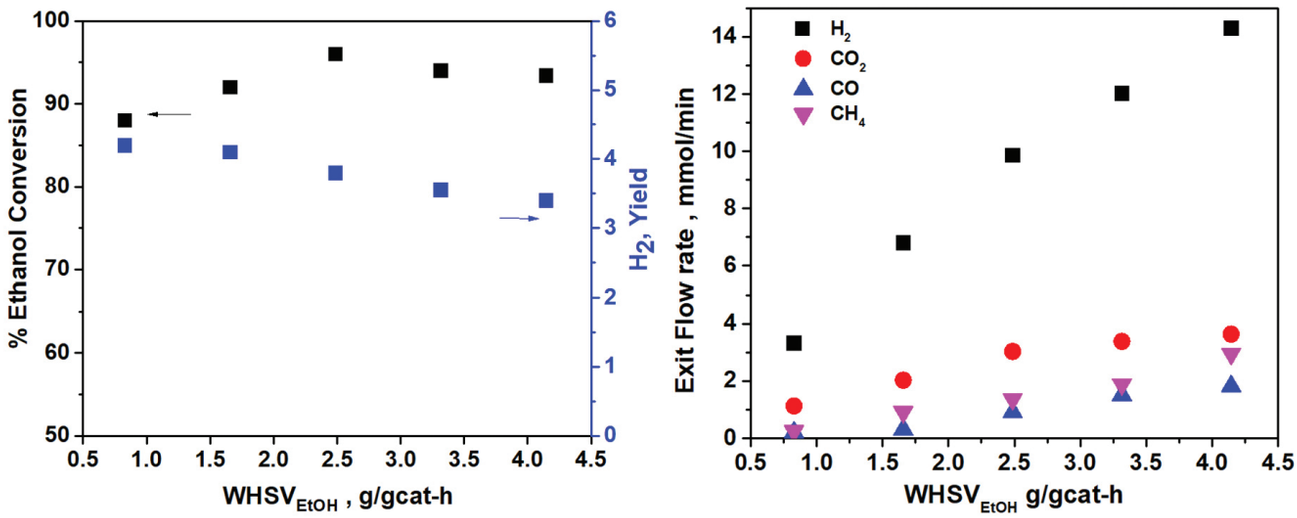


**Figure 5: (a) Effect of WHSV vs ethanol conversion and hydrogen yield, (b) exit flow rate of product@600 °C and 4.5 S/C molar ratio.**

the conversion is the (WGSR), which transforms CO into $CO_2$ and $H_2$. Similarly, an increase in hydrogen yield is also observed as the rise in the S/C ratio reaches a maximum of 4.1. This is because, by lowering carbon deposition and encouraging water-gas shift reactions, greater steam concentrations aid in shifting the equilibrium of the reforming reactions towards the desired products (Alberton et al., 2007).

Figure 6(b) depicts the product flow rate effect on the steam/carbon ratio. As the exit flow rate of hydrogen and $CO_2$ first increases and reaches a maximum of up to 10 mmol/min and 3 mmol/min at an S/C ratio of 4.5. The reason for the trend is that steam availability could not be enough to fully convert ethanol to hydrogen and other required products at lower S/C ratios (Hernández et al., 2010). More steam is available to react with ethanol when the S/C ratio rises, accelerating reforming reactions and boosting the creation of hydrogen and $CO_2$.

The exit flowrate of $CH_4$ shows almost similar trend and observed maximum as 1.5 mmol/min, but in the case of CO, there is a decreasing trend of exit flowrate from 5.9 mmole/min to 0.8 mmole/min as the steam/carbon ratio increases because higher S/C ratios limit the availability of carbon for methanation processes ($CO + 3H_2 \rightarrow CH_4 + H_2O$). Methanation

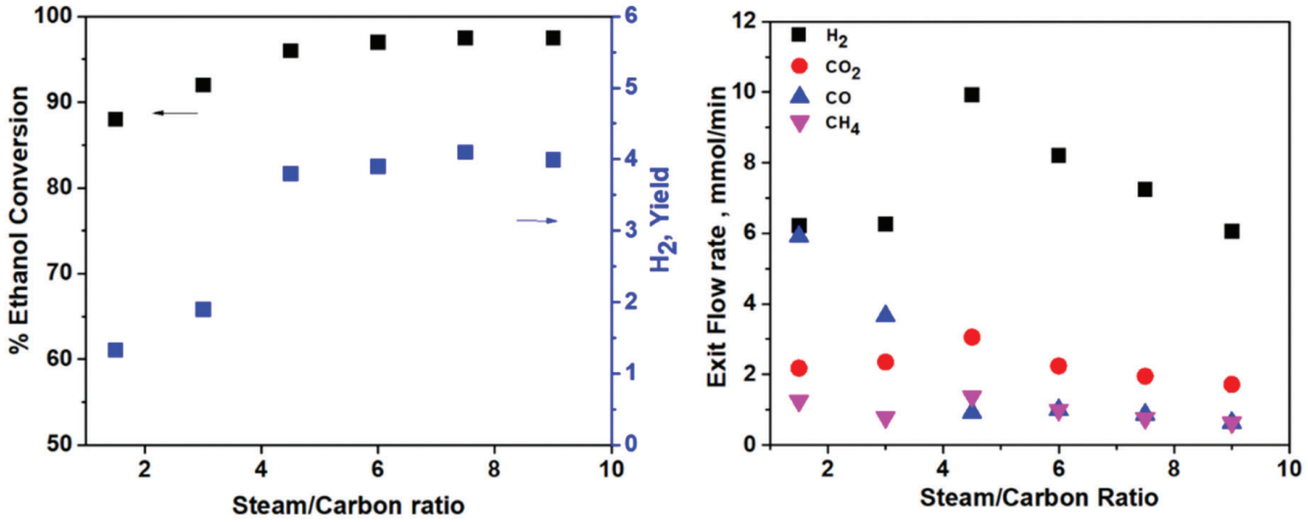


**Figure 6: (a) Effect of steam/carbon ratio vs ethanol conversion and hydrogen yield, (b) exit flow rate of products @600 °C and WHSV-2.5 g/gcat-h.**

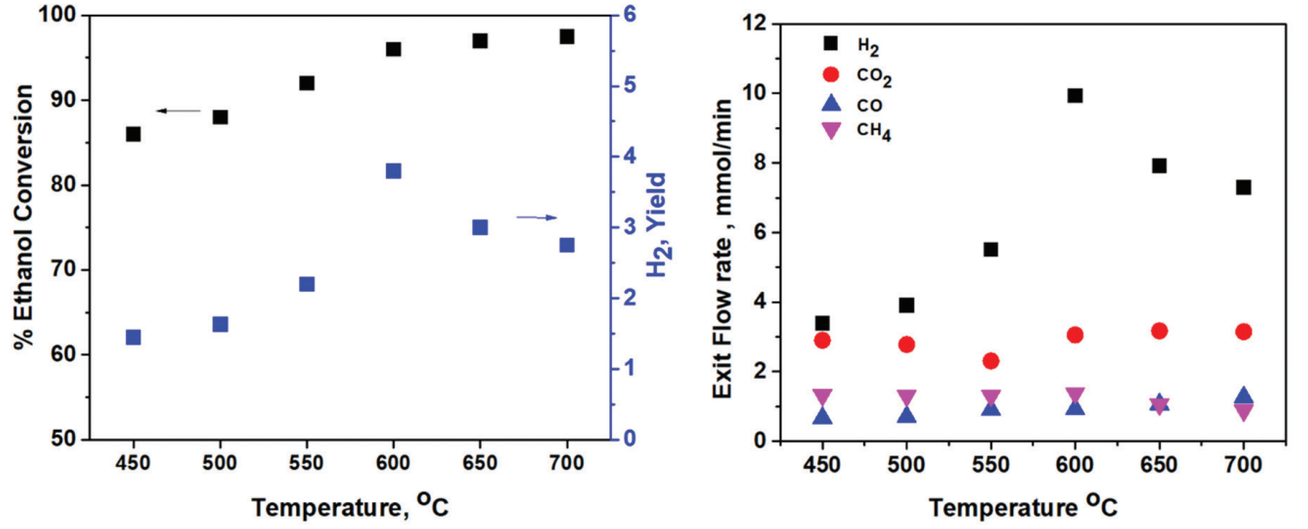


**Figure 7: (a) Effect of temperature vs ethanol conversion and hydrogen yield, (b) exit flow rate of products @600 °C and S/C molar ratio-4.5.**

uses CO and hydrogen to produce methane and water. With fewer accessible carbon atoms due to the greater steam concentration, the methanation reaction is less favourable, resulting in less methane synthesis and, as a result, decreased CO consumption.

**Effect of Temperature**

The temperature effect on ethanol conversion is complex as increasing temperature generally improves conversion rates by speeding up reaction kinetics and promoting thermodynamically favorable events. Figure 7(a) depicts the effect of temperature on ethanol conversion and hydrogen yield. It is observed as the temperature rises, the conversion of ethanol also increases and reaches a maximum of up to 98% (at 700 °C), as increasing the temperature in ethanol steam reforming boosts ethanol conversion by speeding up reaction kinetics, reducing the activation energy barrier, favouring product formation at equilibrium, and improving catalyst activity, thereby increasing the efficiency of ethanol conversion into desired products. But the hydrogen yield rises with increasing reactor temperature and goes maximum as 3.8 mole/mole at 600 ºC and decreases with further increase in temperature.

Figure 7(b) depicts the effect of temperature with exit flowrates of product gases such as $H_2$, $CO_2$, CO, and $CH_4$ and shows that there is an increment in $H_2$ as increasing the temperature and reaching a maximum of 10 mmol/min. As the hydrogen flow rate first increases due to more ethanol molecules activating on the catalyst's surface as more hydrogen formation occurs as temperature increases and the temperature reaches up to optimum condition, a decreasing trend is observed due to the catalyst's deactivation and formation of coke on the surface of the catalyst. CO and $CH_4$ flow rates are quite low, as observed at 0.09 mmol/min and 0.13 mmol/min. Furthermore, $CH_4$ can be consumed by secondary reactions like steam reforming, which further decreases the gas's concentration in the exit stream. A similar trend is observed for $CO_2$, where the exit flow rate remains constant at around 0.30 mmol/min. The formation of $CO_2$ is a major problem for hydrogen yield. Hence the optimum temperature for maximum hydrogen yield is found to be 600 °C

Table 3 compiles the Ni-based catalyst activity in the ethanol steam reforming at 600 °C. The shows a comparative assessment of our catalyst with the reported Ni-based catalyst. The addition of lanthanum significantly increased ethanol conversion and the hydrogen yield at 600 °C in comparison to the other Ni-based catalyst.

**Long-Term Stability Test of Catalyst**

The catalyst (7.5Ni-7.5La/Ce-Zr) was subjected to the long-term stability test at the optimum reaction conditions (600 ºC, S/C: 4.5 and GHSV : 2.5 g/gcat-h). The experiment was conducted for 60 hours, and data were collected every two hours. Figure 8 shows the ethanol conversion with the time on stream. A 4 ~ 5% decrease is observed in the initial 6 hours, and after that, the % ethanol conversion was almost constant. The data suggest that at optimum conditions, the catalyst shows good stability with almost negligible deactivation in the initial 60 hours.

**Table 3: Comparative assessment of the catalyst performance from the literature**

| *Catalyst used* | *Reaction conditions* | *% Ethanol conversion* | *% Hydrogen yield (HY)/ selectivity(S)* | *References* |
|---|---|---|---|---|
| $Ni/Al_2O_3$ | T: 600 ºC, S/C: 16 | 20 | S:48 | (Alberton et al., 2007) |
| $Ni/Ce_{0.6}Zr_{0.4}O_2$ | T: 600 ºC, S/C: 6 | 93 | - | (Trane-Restrup et al., 2013) |
| $Ni/CeO_2$ | T: 600 ºC, S/C: 5.8 | 67 | S: 68 | |
| $Ni/Mg\ Al_2O_4$ | T: 600 ºC, S/C: 6.2 | 73 | S: 70 | |
| $Ni/Ce_{0.74}Zr_{0.26}O_2$ | T: 600 ºC, S/C: 16 | 88 | S: 33 | (Mondal et al., 2015) |
| $Ni\text{-}W/Al_2O_3$ | T: 600 ºC, S/C: 4 | 95 | S: 69 | (Hernández et al., 2010) |
| $Ni/CeO_2$ | T: 600 ºC, S/C: 6, GHSV: 20,000mL/($g_{cat}$ h) | 89 | S: 71 | (Niazi et al., 2020) |
| $Nano\text{-}NiO/SiO_2$ | T: 600 ºC, S/C: 8 | 85 | S:54 | (Bej et al., 2017) |
| 7.5Ni-7.5La/Ce-Zr | At 600 ºC, S/C: 4.5 and GHSV : 2.5 g/gcat-h | 96 | S: 65<br>HY:4.2 | This work |

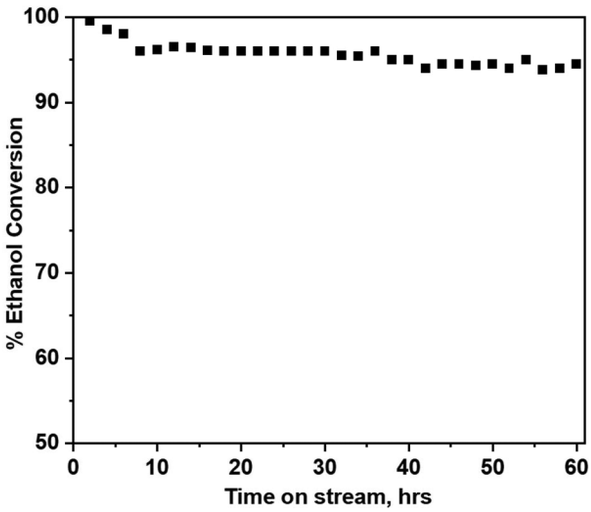


**Figure 8: Stability test of catalyst 7.5Ni-7.5La/Ce-Zrat 600 ℃ and S/C molar ratio-4.5 and GHSV:2.5 g/gcat-h.**

## Conclusions

The effects of various reaction conditions on the performance of 7.5Ni-7.5La/Ce-Zr catalyst in the SRE reaction were examined. The effective parameters such as temperature, S/C ratio, and molar feed flow rate affect the hydrogen yield and conversion. The lanthanum-modified nickel on the $CeO_2$-$ZrO_2$ catalyst was prepared by coprecipitation and impregnation method as the equal weight ratio (7.5wt %). The average particle size of the 7.5Ni-7.5La/$CeO_2$-$ZrO_2$ catalyst is 11.9 nm. The BET investigates the surface area as 41.10 $m^2$/g. As a high surface area accelerates the reaction on its surface, more active sites are involved to accelerate the hydrogen yield.

The catalyst was tested at various temperatures as (400℃ -700 ℃), steam/carbon ratios (1.5- 9), and feed flowrates of 0.8-4.5 g/gcat-h. At 600 ℃, S/C: 4.5 and GHSV: 2.5 g/gcat-h, the optimum ethanol conversion was 96 %, and the hydrogen yield of 4.2. The exit flow rate of hydrogen was observed to be 10 mmol/min at similar conditions. The studies detailed in this report highlight the utilization of 7.5Ni-7.5La/$CeO_2$ -$ZrO_2$ catalyst as a promising technological approach for producing a hydrogen-rich stream through ethanol steam reforming. This process could exhibit high selectivity towards hydrogen production, contingent upon the experimental parameter.

## References

Abd El-Hafiz, D.R. and M.A. Ebiad (2015). A study to develop nano-spray freeze dried Co/Ce–La catalyst for the production of hydrogen from bio-renewable feedstock. *Journal of Natural Gas Science and Engineering*, **27:** 1158-1164. https://doi.org/10.1016/J.JNGSE.2015.09.060

Alberton, A.L., Souza, M.M.V.M. and M. Schmal (2007). Carbon formation and its influence on ethanol steam reforming over Ni/$Al_2O_3$ catalysts. *Catalysis Today*, **123:** 257-264. https://doi.org/10.1016/j.cattod.2007.01.062

Alptekin, F.M. and M.S. Celiktas (2022). Review on catalytic biomass gasification for hydrogen production as a sustainable energy form and social, technological, economic, environmental, and political analysis of catalysts. *ACS Omega*, **7:** 24918-24941. https://doi.org/10.1021/acsomega.2c01538

Bej, B., Bepari, S., Pradhan, N.C. and S. Neogi (2017). Production of hydrogen by dry reforming of ethanol over alumina supported nano-NiO/$SiO_2$ catalyst. *Catalysis Today*, **291:** 58-66. https://doi.org/10.1016/j.cattod.2016.12.010

Calles, J.A., Carrero, A. and A.J. Vizcaíno (2009). Ce and La modification of mesoporous Cu-Ni/SBA-15 catalysts for hydrogen production through ethanol steam reforming. *Microporous and Mesoporous Materials*, **119:** 200-207. https://doi.org/10.1016/j.micromeso.2008.10.028

Frusteri, F., Freni, S., Spadaro, L., Chiodo, V., Bonura, G., Donato, S. and S. Cavallaro (2004). $H_2$ production for MC fuel cell by steam reforming of ethanol over MgO supported Pd, Rh, Ni and Co catalysts. *Catalysis Communications*, **5:** 611-615. https://doi.org/10.1016/j.catcom.2004.07.015

Hernández, I.P., Gochi-Ponce, Y., Contreras Larios, J.L. and A.M. Fernández (2010). Steam reforming of ethanol over nickel-tungsten catalyst. *International Journal of Hydrogen Energy*, **35:** 12098-12104. https://doi.org/10.1016/j.ijhydene.2009.09.069

Li, M., Wang, X., Li, S., Wang, S. and X. Ma (2010). Hydrogen production from ethanol steam reforming over nickel based catalyst derived from Ni/Mg/Al hydrotalcite-like compounds. *International Journal of Hydrogen Energy*, **35:** 6699-6708. https://doi.org/10.1016/j.ijhydene.2010.04.105

Liu, J.Y., Su, W.N., Rick, J., Yang, S.C., Pan, C.J., Lee, J.F., Chen, J.M. and B.J. Hwang (2016). Rational design of ethanol steam reforming catalyst based on analysis of Ni/$La_2O_3$ metal-support interactions. *Catalysis Science and Technology*, **6:** 3449-3456. https://doi.org/10.1039/c5cy00410a

Mondal, T., Pant, K.K. and A.K. Dalai (2015). Oxidative and non-oxidative steam reforming of crude bio-ethanol for hydrogen production over Rh promoted Ni/$CeO_2$-$ZrO_2$ catalyst. *Applied Catalysis A: General*, **499:** 19-31. https://doi.org/10.1016/j.apcata.2015.04.004

Mortensen, P.M. and I. Dybkjær (2015). Industrial scale experience on steam reforming of $CO_2$-rich gas. *Applied Catalysis A: General*, **495:** 141-151. https://doi.org/https://doi.org/10.1016/j.apcata.2015.02.022

Ni, M., Leung, D.Y.C. and M.K.H. Leung (2007). A review on reforming bio-ethanol for hydrogen production. *International Journal of Hydrogen Energy*, **32:** 3238-3247. https://doi.org/10.1016/j.ijhydene.2007.04.038

Niazi, Z., Irankhah, A., Wang, Y. and H. Arandiyan (2020). Cu, Mg and Co effect on nickel-ceria supported catalysts for ethanol steam reforming reaction. *International Journal of Hydrogen Energy*, **45:** 21512-21522. https://doi.org/10.1016/j.ijhydene.2020.06.001

Ong, J.L., Loy, A.C.M., Teng, S.Y. and B.S. How (2022). Future paradigm of 3D printed Ni-based metal organic framework catalysts for dry methane reforming: Techno-economic and environmental analyses. *ACS Omega*, **7:** 15369-15384. https://doi.org/10.1021/acsomega.1c06873

Phaahlamohlaka, T.N., Kumi, D.O., Dlamini, M.W., Forbes, R., Jewell, L.L., Billing, D.G. and N.J. Coville (2017). Effects of Co and Ru intimacy in Fischer-Tropsch catalysts using hollow carbon sphere supports: Assessment of the hydrogen spillover processes. *ACS Catalysis*, **7:** 1568-1578. https://doi.org/10.1021/acscatal.6b03102

Quan, C., Xu, S. and C. Zhou (2017). Steam reforming of bio-oil from coconut shell pyrolysis over Fe/olivine catalyst. *Energy Conversion and Management*, **141:** 40-47. https://doi.org/10.1016/j.enconman.2016.04.024

Sanchez-Sanchez, M.C., Yerga, R.M.N., Kondarides, D.I., Verykios, X.E. and J.L.G. Fierro(2010). Mechanistic aspects of the ethanol steam reforming reaction for hydrogen production on Pt, Ni, and PtNi catalysts supported on $\gamma$-$Al_2O_3$. *Journal of Physical Chemistry A*, **114:** 3873-3882. https://doi.org/10.1021/jp906531x

Trane-Restrup, R., Dahl, S. and A.D. Jensen (2013). Steam reforming of ethanol: Effects of support and additives on Ni-based catalysts. *International Journal of Hydrogen Energy*, **38:** 15105-15118. https://doi.org/10.1016/j.ijhydene.2013.09.027

Vizcaíno, A.J., Carrero, A. and J.A. Calles (2007). Hydrogen production by ethanol steam reforming over Cu-Ni supported catalysts. *International Journal of Hydrogen Energy*, **32:** 1450-1461. https://doi.org/10.1016/j.ijhydene.2006.10.024

Xiao, Z., Wu, C., Wang, L., Xu, J., Zheng, Q., Pan, L., Zou, J., Zhang, X. and G. Li (2021). Boosting hydrogen production from steam reforming of ethanol on nickel by lanthanum doped ceria. *Applied Catalysis B: Environmental*, **286:** 119884. https://doi.org/10.1016/j.apcatb.2021.119884